Evaluation of Head Defect Images of Railway Rails in Laser Scatterometry

Piotr LESIAK[1], Aleksander SOKOŁOWSKI[2]

Summary

The images of head checking faults of railway rails have been examined by laser scattering method. The studies used the functions of similarity and distance, both for binary images and multi-level quantized ones. The analysis was performed on the basis of numerical calculations, experimentally determined images of samples of these defects. These type of functions have proven extremely useful in evaluating these faults and can be used to classify them.

Keywords: railway rails, head checking, laser scatterometry method, similarity functions, distance functions

1. Introduction

Rolling Contact Fatigue (RCF) has a significant impact on railway traffic safety. Therefore complex phenomena accompanying these defects are analyzed in the framework of the research program of the European Railway Research Institute [2] and to unify the terminology (UIC Rail Defect Catalog) [21].

A representative example of this disadvantage is the head checking (HC) defect, which results from the fatigue of the rolling surface material of the rail when the rail is subjected to cyclic loading due to the pressure of the wheels of the passing train [4, 22]. As a result of this pressure, repeated subsurface stresses occur and consequently microcracks. The depth of these microcracks varies from a millimeter to a few millimeters. They develop into the depths of the rails until critical dimensions are reached, leading to cracks and fractures [3, 17-20]. This results in numerous derailments and accompanying serious consequences.

Therefore, it is very important to thoroughly examine these defects, possibly by various methods. It can be mentioned here ultrasonic method as the basic used by PKP PLK S.A. [7], Method of Eddying Current (ED) [8, 16], Magnetic Flux Leakage (MFL) [8] or Method of Metal Magnetic Memory (MMM) [6]. Neither method is perfect, hence the search for alternative solutions.

Therefore, the authors investigate the disadvantages of contact and tension of railway rails, for several years they have been testing optical methods, including the method of laser scatterometry [9, 11-14].

Figure 1 shows the principle of measurement with this method. It consists of scanning the rail surface with a laser beam and recording the reflected beam or diffuse beam [9].

The beam of light emitted by the laser is directed at an angle to the running surface of the rail. The detector, when recording the image by the camera, records the laser light distribution. When the surface of the rails is perfectly smooth, there is a mirror image, whereas when the surface contains surface defects, the laser beam is scattered.
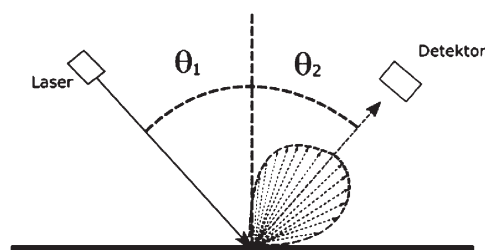

Fig. 1. The principle of measurement of surface defects of railway rails using the method laser scattering

2. Exemplary results of tests of HC defect images

The tests were carried out with rail fragments removed from the railway track with real defects HC and the standard of these defects, made mechanically (high power laser cutting) on the rolling surface of the rail head. Figure 2 shows samples of HC defects, numbered 1 to 5, and HC12, HC13 and HC14 defect standards, respectively, in widths, 0.65, 0.7 and 0.75 mm.

[1] PhD DSc. Ing.; University of Economics and Innovation in Lublin, Faculty of Transport and Computer Science; e-mail: piotr.lesiak@wsei.lublin.pl.
[2] PhD.; Rzeszow University of Technology, Department of Management, e-mail: alex5@prz.edu.pl.
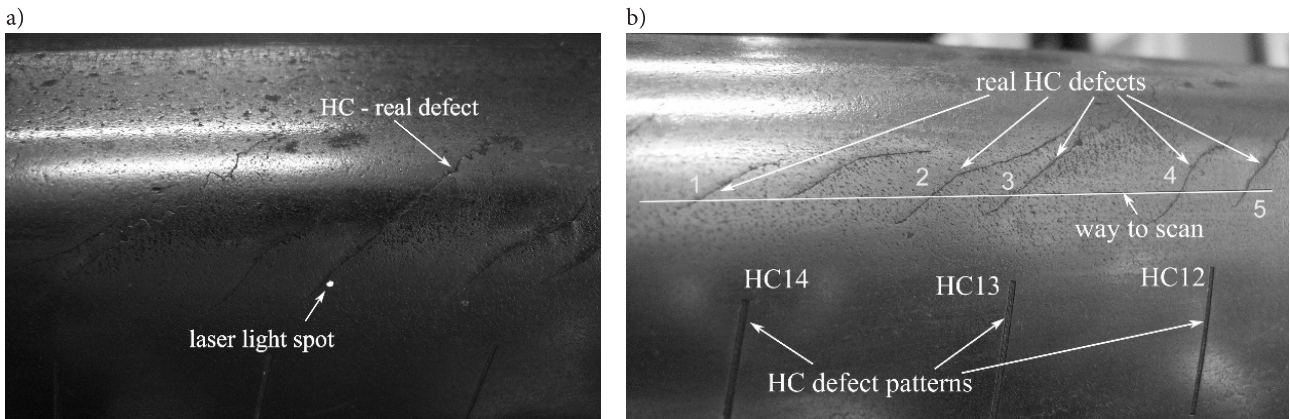
a)

b)

Fig. 2. Rail with patterns and real defects HC: a) laser spot in the area of real defects, b) the way of scanning real defects from 1 to 5 and c) HC defect patterns

The images in Fig. 3 correspond to the laser light distribution from the HC defects shown in Fig. 2b, numbered 1 to 5. There is a superposition of the reflection diffused from the defect and the mirror from the contiguous surface of the rail.

Similar image registrations are shown in Figure 4. This time, they refer to the HC flaw patterns shown in Figure 2b.

Fig. 5 presents the images of rolling surfaces of railway rails obtained from areas where defects are not present. There is also superposition of mirrored and scattered reflections. Mirror reflection results from the relative smoothness of the rail. The dispersion reflection results from the fact that theoretically ideal from the operational point of view the rolling surface of the rail does not constitute a physical mirror.

a)   b)   c)   d)   f)
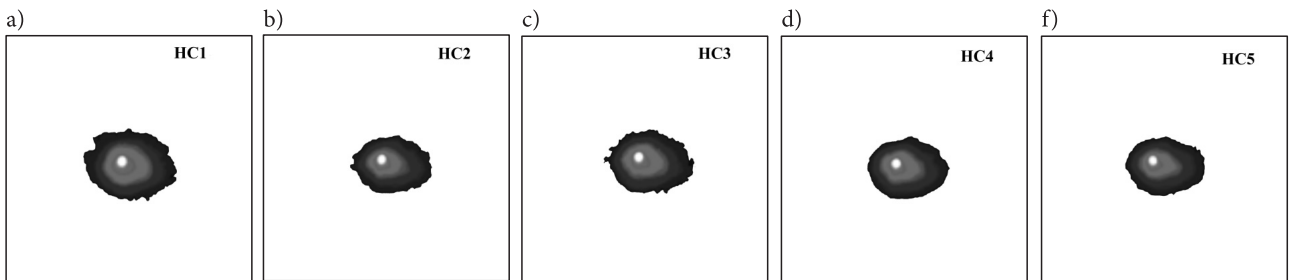
HC1   HC2   HC3   HC4   HC5

Fig. 3. The images of real defects obtained by the laser scattering method, on the laser scanning path, shown in Fig. 2. Figures a), b), c), d) and e) correspond to the points 1, 2, 3, 4 and 5 of Fig. 2b
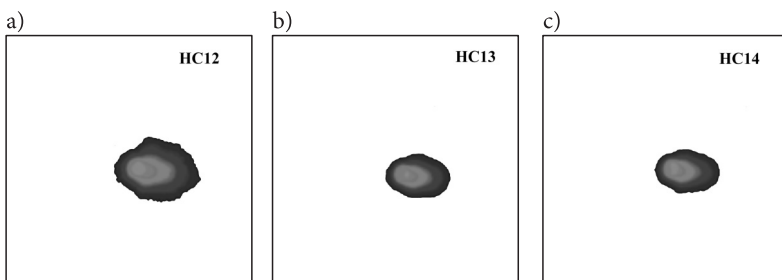
a)   b)   c)

HC12   HC13   HC14

Fig. 4. Pictures of HC defect patterns shown in Fig. 2b corresponding to the HC12, HC13 and HC14 patterns
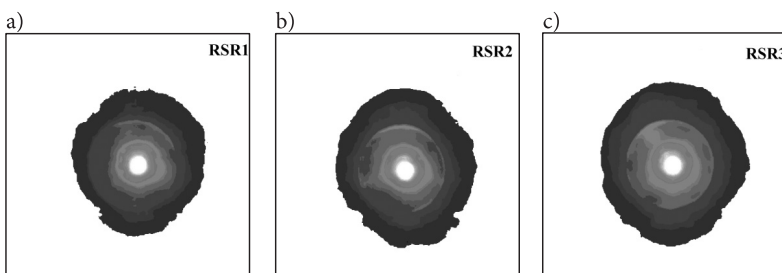
a)   b)   c)

RSR1   RSR2   RSR3

Fig. 5. The images of rolling surfaces of the railway rails

3. Similarity functions and distance functions of HC images

Similarity functions and distance functions have been used to evaluate the defects of HC. A measure of the similarity between two images, such as images obtained by laser sketching, can be defined as a function f with properties:

$$f : A(x,y) \sim B(x,y) \to [0,1], \qquad (1)$$

i.e. converting two objects (images) A and B into the interval [0, 1]. If both objects are identical, the value is 1. The most commonly used in literature for similarity functions are correlation functions and Tanimoto functions [10] and for the binary images, the Jaccard index [1] and the Sørensen coefficient [15]. The correlation function is defined as [10-12].

$$F_C = \frac{\mathbf{w}^T \tilde{\mathbf{w}}}{\|\mathbf{w}\| \|\tilde{\mathbf{w}}\|}, \qquad (2)$$

where: $\mathbf{w}$ and $\tilde{\mathbf{w}}$ is a two-dimensional matrix containing the pixel values of the two images being compared, $\|\mathbf{w}\|$ means the module of vector $\mathbf{w}$ (image). Its values are in the range of [0, 1].

The Tanimoto function is defined as [10-12]:

$$F_{TA} = \frac{\mathbf{w}^T \tilde{\mathbf{w}}}{\mathbf{w}^T \mathbf{w} + \tilde{\mathbf{w}}^T \tilde{\mathbf{w}} - \mathbf{w}^T \tilde{\mathbf{w}}}. \qquad (3)$$

For binary images, the Jaccard index is defined as follows [1]:

$$F_{JC} = \frac{|A \cap B|}{|A \cup B|}, \qquad (4)$$

where: symbol $\cap$ denotes conjunction and symbol $\cup$ denotes alternation of two sets.

In turn, the Sørensen coefficient [15], although mainly used to evaluate the similarity of the two samples and created by the botanist Thorvald Sørensen in 1948, can also be applied in other areas. It is similar to the Jaccard index:

$$F_{SO} = \frac{2|A \cap B|}{|A + B|}, \qquad (5)$$

where: symbol + means the set of all samples from both A and B sets.

It can be also used the distance functions G or metrics, with a relation $F = 1 / G$ if G is different from zero. The distance function (or metric) on the set X is called the function $d : X \times X \to \mathbf{R}$ satisfying the following conditions:

1. Zero condition
   $\forall_{x,y \in X} d(x,y) = 0$ if and only if $x = y$,
2. Condition of symmetry $\forall_{x,y \in X} d(x,y) = d(y,x)$,
3. Triangle condition
   $\forall_{x,y,z \in X} d(x,y) \leq d(x,z) + d(y,z)$.
   Pair (X, d) is called a metric space.

Sometimes it is considered the so-called pseudo-metric spaces, where in the first condition the existence of other objects with a „zero distance". Euclidean metrics are often used in research work [10]:

$$d_{EU}(\mathbf{w}, \tilde{\mathbf{w}}) = \frac{\sqrt{\sum_{i=1}^{N}(w_i - \tilde{w}_i)^2}}{\|\tilde{\mathbf{w}}\|}, \qquad (6)$$

where: N is the number of elements of the set X. Another metric that is often used is the Minkowski metric [10]:

$$d_M(\mathbf{w}, \tilde{\mathbf{w}}) = \left(\sum_{i=1}^{N} |w_i - \tilde{w}_i|^m \right)^{\frac{1}{m}}. \qquad (7)$$

Minkowski's metric can be considered as an extension of Euclidean's metric.

One pseudo-metric can be defined using the cardinal sinc function so-called sinc function, especially used in optics [5], i.e.

$$\text{sinc}(x) = \frac{\sin(\pi x)}{\pi x}. \qquad (8)$$

It can be selected the interval $(-p, p]$ and specify the pseudo-metric in this field:

$$d_{SI}(\mathbf{w}, \tilde{\mathbf{w}}) = \begin{cases} \sum_{i=1}^{N} \left[1 - \text{sinc}(\lambda_i |w_i - \tilde{w}_i|) \right] \text{ dla } |\lambda_i(w_i - \tilde{w}_i)| < \pi, \\ 0 \text{ dla } |\lambda_i(w_i - \tilde{w}_i)| \geq \pi. \end{cases}$$

$$(9)$$

This interval as a domain of a function is commonly used in case of Fourier transform.

4. Numerical calculations

The similarity functions and metrics defined in point 3 were used for numerical calculations of defects of HC Fig. 3, their patterns, Fig. 4, and the images of rolling surfaces of rails, Fig. 5. First, results are presented for the binary images.

Table 1 presents the results obtained when comparing the images shown in Figure 3. Both the Jaccard

index and the Sørensen coefficient are designed to emphasize the similarity between the two samples. As can be seen from the calculations, the similarity of the individual HC defects is significant with a slight advantage of the Sørensen coefficient. For example, binary HC4 and HC5 images have been used. In this case, Jaccard index is 0.84, while Sørensen coefficient – 0.91, which means high similarity of images of these defects.

Similarly, Table 2 shows the results for the image patterns in Fig. 4. Here too the same similarity measures were used, as in Table 1, and trends are similar to those for real defects. The width of their cuts is recognized.

Table 3 shows the similarity between the two types of images in Figures 3 and 4. The obtained values show a slight similarity between the actual HC defects and their patterns, i.e. the two groups of images differ significantly. The reasons should probably be seen

in too wide a pattern width (point 2), with the hairspace width of the real defects. In the images of real defects clearly visible reflection of the mirror, while in the images of defect patterns dominate the dispersion component.

Table 4 allows us to assess how the actual HC defects are detected against the rolling surface of the rails, RSR1 (Fig. 5a), RSR2 (Fig. 5b) and RSR3 (Fig. 5c). Jaccard's index performs better than this because the similarities are significantly lower than for the Sørensen coefficient. It is sufficient to classify here a simple threshold criterion. It should be noted that the more the surface of the rail will approximate the mirror surface, the smaller the coefficients will be, and the easier classification.

Further calculations involve quantized images with a resolution of 8 bits, i.e. 256 levels. Two simi-

Table 1

The results obtained for the images in Figure 3 for the Jaccard index and the Sørensen coefficient

Jaccard index							Sørensen coefficient				
	HC1	HC2	HC3	HC4	HC5			HC1	HC2	HC3	HC4	HC5
HC1	1	–	–	–	–		**HC1**	1	–	–	–	–
HC2	0.71	1	–	–	–		**HC2**	0.83	1	–	–	–
HC3	0.78	0.79	1	–	–		**HC3**	0.88	0.88	1	–	–
HC4	0.81	0.76	0.72	1	–		**HC4**	0.88	0.87	0.84	1	–
HC5	0.72	0.77	0.77	0.84	1		**HC5**	0.83	0.87	0.87	0.91	1

Table 2

The results obtained for the images in Figure 4 for the Jaccard index and the Sørensen coefficient

Jaccard index					Sørensen coefficient			
	HC12	HC13	HC14			HC12	HC13	HC14
HC12	1	–	–		**HC12**	1	–	–
HC13	0.62	1	–		**HC13**	0.76	1	–
HC14	0.78	0.66	1		**HC14**	0.87	0.79	1

Table 3

Results from Figures 3 and 4 for the Jaccard index and Sørensen coefficient

Jaccard index							Sørensen coefficient				
	HC1	HC2	HC3	HC4	HC5			HC1	HC2	HC3	HC4	HC5
HC12	0.29	0.32	0.29	0.30	0.27		**HC12**	0.45	0.48	0.45	0.47	0.42
HC13	0.28	0.32	0.25	0.30	0.24		**HC13**	0.43	0.48	0.40	0.46	0.39
HC14	0.32	0.40	0.32	0.35	0.31		**HC14**	0.49	0.57	0.48	0.52	0.47

Table 4

Results for the two types of images in Figures 3 and 5

Jaccard index							Sørensen coefficient				
	HC1	HC2	HC3	HC4	HC5			HC1	HC2	HC3	HC4	HC5
RSR1	0.38	0.27	0.32	0.30	0.27		**RSR1**	0.55	0.43	0.49	0.47	0.42
RSR2	0.33	0.24	0.28	0.26	0.23		**RSR2**	0.49	0.38	0.44	0.42	0.38
RSR3	0.28	0.20	0.24	0.22	0.20		**RSR3**	0.44	0.33	0.39	0.37	0.33

larity functions, Tanimoto function, correlation function, and three distance functions are used: Euclidean, Minkowski and pseudo-distance based on the definition of the sinc function. They gave values of 0.48 and 0.83 for the highest values, and 0.26 and 0.70 for the smallest values. Limited to the evaluation of HC defects on the rolling surface.

Table 5 shows the similarity of images as in Table 4. The function values for each of the rolling surfaces of the rails have a smaller scatter for each HC defect, especially for the correlation function, as compared to the binary images (Table 4). This demonstrates the less distinction of their width. In addition, the surface of the RSR3 rail is characterized by the best mirror image of the light, as it has the relatively lowest values of proximity.

Table 6 contains the values of Euclidean and Minkowski's distance functions and sinc pseudo-distances for the images of the defects and patterns of Figures 3 and 4, respectively, and the rolling surfaces of Figure 5. In the case of the Euclidean distance function, the Minkowski function and pseudo-distance sinc function, the values of these functions depend on the normalization of these functions. If the functions are similar, the values of the distance functions are close to zero. In the case of distinctly different functions, the distance function can take a value greater than 1, which is evident in the Minkowski function.

The results obtained in the order of greatest distances were 0.81, 1.03 and 0.88, and for the smallest 0.68, 0.73 and 0.85. For the Euclidean function, this gives a difference of about 0.13 for the Minkowski function – about 0.3 a for the pseudo-distance sinc – 0.03. So the distance functions shown at work give similar results to the same images.

The sinc function does not recognize the widths of real defects, just like the patterns. Its values for both types of images are similar, so the suitability in the classifier is small.

5. Conclusion

The evaluation of the images of HC rail rails defects investigated by laser scatterometry has been performed. For this purpose, the functions of similarity and distance have been used. The results of the study refer to the images of real defects, their patterns and the rolling surfaces of the rail. Images of real defects have similar parameters. In contrast, HC1 and HC2 images are 0.71 and 0.83, respectively. They are the least similar to each other. The images of real defects and rolling surfaces have been compared by means of Tanimoto and Correlation functions. These results show that the images are clearly separated from each other in terms of similarity.

Table 5

Results for the Tanimoto similarity and correlation function of the two types of images shown in Figures 3 and 5

Tanimoto function						Correlation function					
	HC1	HC2	HC3	HC4	HC5		HC1	HC2	HC3	HC4	HC5
RSR1	0.48	0.35	0.41	0.38	0.34	**RSR1**	0.83	0.75	0.75	0.82	0.79
RSR2	0.43	0.31	0.36	0.34	0.30	**RSR2**	0.79	0.70	0.72	0.76	0.74
RSR3	0.43	0.26	0.31	0.29	0.26	**RSR3**	0.75	0.66	0.68	0.72	0.70

Table 6

Results for normalized distance functions of Euclidean, Minkowski and pseudo-distance sinc for the images in Figures 3, 4 and 5

Euklidean distance function						Minkowski's distance function					
	HC1	HC2	HC3	HC4	HC5		HC1	HC2	HC3	HC4	HC5
RSR1	0.68	0.75	0.72	0.74	0.77	**RSR1**	0.73	0.80	0.78	0.80	0.83
RSR2	0.77	0.79	0.76	0.77	0.79	**RSR2**	0.82	0.91	0.88	0.88	0.92
RSR3	0.74	0.81	0.78	0.80	0.79	**RSR3**	0.93	1.02	0.99	1.00	1.03

Pseudo-distance sinc function						Pseudo-distance sinc function			
	HC1	HC2	HC3	HC4	HC5		HC12	HC13	HC14
RSR1	0.85	0.88	0.86	0.86	0.87	**RSR1**	0.82	0.88	0.89
RSR2	0.87	0.88	0.87	0.87	0.88	**RSR2**	0.87	0.88	0.89
RSR3	0.86	0.87	0.87	0.87	0.88	**RSR3**	0.89	0.88	0.89

The distance functions described by Euclidean, Minkowski and pseudo-sinc functions were also used to compare the defect images and their patterns against the rolling surface (Table 6). The pseudo-distance sinc function gives the most compact results for defect images, similarly to their patterns. Therefore its usefulness in comparison with other functions is small.

When analyzing images of HC defects and rolling surfaces, all the results of the investigated functions give the correct results, except for the pseudo-distance sinc. Similar results can be obtained for defect patterns and rolling surfaces. On the other hand, images of defect patterns are not very similar to real HC defects, which is justified in the text.

In order to accurately assess the entire length of HC defects, it would be necessary to scan them with a laser beam in multiple transverse sections. The resulting images should then be superposed for further analysis. This will be the subject of further research by the authors.

In addition, such studies should concern a larger population of rails samples. This will allow for the proper selection of defect classifiers, based not only on threshold values but more advanced, using intelligent algorithms [10].

Literature

1. Albatineh A.N., Niewiadomska-Bugaj M.: *Correcting Jaccard and other similarity indices for chance agreement in cluster analysis*. Advances in Data Analysis and Classification, Springer 2011, Vol. 5, Issue 3, pp 179–200.
2. Cannon D.F., Pradier H.: *Rail rolling contact fatigue Research by the European Rail Research Institute*. // Wear, 191, (1996), pp. 1–13.
3. Edel K.O.: *Aus der Rollkontaktermüdung resultierende Lebensdauer von Eisenbahnschienen*. Technische Universität Berlin, Eisenbahnwesen-Seminar, 12. Juni 2017 (Vortragsmanuskript) [online], https://www.ews.tu-berlin.de/fileadmin/fg98/aushaenge/2017-sose/2017-06-12_EWS_Edel_Rollkontakterm%C3%BCdung.pdf, [acces: 10 marca 2017].
4. Ekberg A., Kabo E.: *Fatigue of railway wheels and rails under rolling contact and thermal loading-an overview*, Wear 258 (2005), pp. 1288–1300.
5. Gniadek K.: *Optyczne przetwarzanie informacji*, PWN, Warszawa, 1992.
6. Lesiak P., Bojarczak P.: *Application of neural classifier to railway flaw detection in the method of metal magnetic memory*. The 6 th International Conference „Environmental Engineering", Selected Papers Vol. 2, May 26-27, 2005, Vilnius, Lithuania, pp. 744-747.
7. Lesiak P.: *Diagnostic sensitivity of ultrasonic mobile flaw detection of head checking type flaws in railway rails*, Diagnostyka, Vol.2, No 2, 2008, pp. 37–40.
8. Lesiak P.: *Diagnostic technology of contact-stress flaws such as head checking in railway rails,* Technical University of Radom, Monograph No 121, 2008, pp. 187–198.
9. Lesiak P., Szumiata T.: *Skaterometria laserowa wad head checking w szynach kolejowych*. PAKGOŚ nr 2/2010, s. 25–28.
10. Lesiak P., Bojarczak P.: *Przetwarzanie i analiza obrazów w wybranych badaniach defektoskopowych,* Monograficzna seria wydawnicza Biblioteka Problemów Eksploatacji, Wydawnictwo Naukowe Instytutu Technologii Eksploatacji – PIB, Radom 2012, s. 185.
11. Lesiak P., Wlazło M.: *Badania wad head checking w szynach kolejowych metodą optyczną,* Prace Naukowe Politechniki Warszawskiej, Transport, z.104, 2014, s. 33–42.
12. Lesiak P., Wlazło M.: *Wizualizacja i analiza obrazów wad head checking w szynach kolejowych badanych metodą skaterometrii laserowej*, Logistyka 6/2014 (CD), s. 6637–6642.
13. Lesiak P., Sokołowski A., Wlazło M.: *Dwuwymiarowa funkcja korelacji obrazów wad typu squat w diagnostyce szyn kolejowych metodą skaterometrii laserowej*, Technika Transportu Szynowego, No 7/8, 2016, s. 24–29.
14. Lesiak P., Sokołowski A., Wlazło M.: *Cross-correlation function in identifying head checking defects of the railway rails,* Diagnostyka Vol.18, No 2, 2017, pp. 65–73.
15. Looman J., Campbell J.B.: *Adaptation of Sørensen's K (1948) for estimating unit affinities in prairie vegetation*, Ecology, Vol. 41, No.3, Wiley 1960, pp. 409-416.
16. Popović Z., Brajović L., Lazarević L., Milosavljević L.: *Rail defects head checking on the Serbian Railways*, Tehnički vjesnik 21, 1(2014), pp. 147–153.
17. *Rail Defects Handbook. Some Rail Defects, their Characteristics, Causes and Control.* Engineering Practices Manual, Civil Engineering, Australian Rail Track Corporation, Issue A, Revision 0, March 2006.
18. *Rail Defects Handbook* TMC 226, RailCorp Engineering Manual – Track. Version 1.2, Issued June 2012.
19. *Research Programme Engineering. Management and Understanding of Rolling Contact Fatigue.* WP1: Mechanisms of Crack Initiation. WP2: Crack Growth. Literature Survey, Rail Safety and Standards Board, © Copyright 2006.
20. *Rolling Contact Fatigue in Rails; a Guide to Current Understanding and Practice*, Railtrack PLC Guidelines: RT/PWG/001, Issue 1, 2001.(13).
21. *UIC Code 712 Rail Defects / UIC International Union of Railways*, Paris, 2002.
22. Vidaud M., Zwanenburg W.J.: *Current situation on rolling contact fatigue – a rail wear phenomena.* 9th Swiss Transport Research Conference, Sept 9–11, 2009.

Ocena obrazów wad szyn kolejowych typu *head checking* w badaniach metodą skaterometrii laserowej

Streszczenie

Dokonano oceny obrazów wad szyn kolejowych typu *head checking*, zbadanych metodą skaterometrii laserowej. W badaniach wykorzystano funkcje podobieństwa i odległości, zarówno dla obrazów zbinaryzowanych, jak i skwantowanych wielopoziomowo. Analizę przeprowadzono na podstawie obliczeń numerycznych, wyznaczonych doświadczalnie obrazów próbek tych wad. Funkcje tego typu okazały się przydatne w ocenie tych wad i mogą być wykorzystywane do ich klasyfikacji.

Słowa kluczowe: szyny kolejowe, wady *head checking*, metoda skaterometrii laserowej, funkcje podobieństwa i odległości

Оценка изображений дефектов рельсов типа head checking в исследованиях при использования метода лазерной скаттерометрии

Резюме

В статье была проведена оценка образцов дефектов железнодорожных рельсов типа head checking, тестированных методом лазерной скаттерометрии. В исследовании были использованы функции сходства и расстояния, так для бимодальных образцов как и образцов многоуровненно квантованых. Анализ был проведен на основании цифровых вычислений, определенных экспериментально образцов этих дефектов. Этого типа функции показались черезвычайно полезными для оценки этих дефектов и могут быть использован для их классификации.

Ключевые слова: рельсы, дефекты head checking, метод лазерной скаттерометрии, функции сходства и расстояния